Development of an analytical uncertainty model for ship-based lidar measurements

Journal of Physics: Conference Series **2362** (2022) 012034 doi:10.1088/1742-6596/2362/1/012034

Development of an analytical uncertainty model for ship-based lidar measurements

H Rubio and J Gottschall

Fraunhofer Institute for Wind Energy Systems IWES, 27572 Bremerhaven, Germany

E-mail: hugo.rubio@iwes.fraunhofer.de

Abstract.

Ship-based lidar systems are a cost-efficient alternative for retrieving highly-reliable offshore wind data. However, the non-stationary nature of ship-mounted lidars hinders the comparison against reference datasets and, therefore, a straightforward characterization of the uncertainty levels associated with these sorts of measurements. For this reason, in this paper we have set up and report an analytical model for estimating the uncertainties of ship-based lidar measurements. The model follows the standard uncertainty propagation method considering the relevant parameters for assessing the wind speed from pulsed Doppler-lidar observations, such as the half cone opening angle, the radial velocity estimation, or the lidar beams' orientations. Additionally, the derivation of the presented uncertainty model contemplates the technology-specific variables and considerations like the ship linear velocity or tilting, as well as the implementation of a motion correction algorithm.

1. Introduction

Offshore sites have become of great interest for installing new wind farms. Compared to onshore locations, they offer generally higher mean wind speeds, less temporal and spatial wind variations, and a significant higher potential for bigger projects. However, the development of new wind farms requires highly-reliable in-situ observations for the accurate characterization of local wind conditions. For this purpose, remote sensing technology, and in particular buoy-based floating lidar systems, have emerged as an economically attractive and more flexible alternative to traditional meteorological masts [1, 2].

Ship-based lidar systems are an additional type of floating lidar technology [3, 4]. Their rather simple setup and easy maintenance help to reduce the costs and complexity of offshore measurement campaigns. Furthermore, the constant translation of the ship allows characterizing wind resources along large regions of interest including deep waters sites. Although ship-mounted lidars are still a novel technology within the wind energy industry, previous studies have already shown a promising agreement with fixed measurement devices [5, 6], as well as the applicability of these sorts of observations for different purposes such as the evaluation of low-level jets [7, 8], wind farm wake characterization [5], or the validation of numerical models [3, 9].

Thanks to the execution of validation campaigns against met mast-mounted sensors, buoy-based lidars have demonstrated their performance in agreement with the accuracy standards used by industry [10, 2]. Nevertheless, the non-stationary nature of ship-mounted devices complicates the availability of reference data for validation purposes, and therefore, hinders the further

understanding of the uncertainty level associated with this technology and the development of a reproducible methodology for the employment of these observational data.

As an attempt to address this challenge, this paper presents the development of an analytical uncertainty model that, to the authors knowledge, is the first of its kind for estimating the uncertainty levels associated with ship-based lidar measurements. For this, the law of propagation of uncertainty [11] has been used, taking into consideration the relevant parameters involved in the retrieval of wind speeds from ship-based lidar observations, as well as a motion correction algorithm for the decontamination of measurements from motion effects. This way, we aim to tentatively answer the following research questions:

(i) How accurate are ship-based lidar measurements?
(ii) What is the sensitivity of the measurements to different external and internal parameters?
(iii) How can we optimize the technology setup to reduce the associated uncertainties?

This paper is organized as follows: Section 2 describes in detail the methodology applied for the derivation of the uncertainty model. Firstly, it presents the lidar device and the equations for the retrieval of wind speeds from lidar observations. Later, we derive the uncertainties of the motion-affected radial velocities retrieved by ship-mounted lidars. Then, we introduce the motion correction algorithm and use the law of propagation of uncertainty for deriving the wind speed and direction uncertainties. The results of the model are shown and discussed in Section 3 and we conclude the findings of this study in Section 4.

2. Methodology

2.1. Radial velocity retrievals from non-static lidars

The uncertainty model developed in this study assumes the employment of a pulsed Doppler lidar for the retrieval of wind speed and direction observations. Doppler wind lidars provide radial wind velocity measurements by detecting the Doppler shift in the backscattered light. These radial retrievals are proportional to the projection of the wind speed on the lidar beam direction, so-called line of sight (LoS), and can be related to the wind speed vector $\vec{u}_{wind}$ as:

$$v_{radial} = \vec{n} \cdot \vec{u}_{wind} = \begin{pmatrix} \sin(\theta)\cos(\varphi) \\ \sin(\theta)\sin(\varphi) \\ \cos(\theta) \end{pmatrix} \cdot \begin{pmatrix} u \\ v \\ w \end{pmatrix} \tag{1}$$

where $\vec{n}$ is a unit vector describing the geometry of the scanning lidar beams, defined by the half cone opening angle θ and the azimuth angle φ (see Figure 1a for illustration).

Unlike fixed lidar devices, ship-mounted lidars are affected by the motions of the vessel with 6 degrees of freedom, as illustrated in Figure 1b. Three degrees of freedom for rotational motions around the three coordinates axes (yaw γ – rotation around the vertical axis, measured clockwise; pitch δ – rotation around the west-east axis; and roll β – rotation around the north-south axis) and three linear motions along those same axes (heave, sway and surge). These motions impact the lidar coordinate system, and therefore, the retrieved radial velocity accounting for the ship motions can be mathematically expressed as:

$$v_{radial}^{motion} = R_{rot} \cdot v_{radial}^{wind} - R_{rot} \cdot v_{radial}^{ship} \tag{2}$$

where $R_{rot}(\gamma, \delta, \beta)$ is the rotation matrix considering the ship tilting around the three coordinate axis and v_{radial}^{ship} is the projection of the ship linear velocity on the lidar beam LoS, defined as:

$$v_{radial}^{ship} = \vec{n} \cdot \vec{u}_{ship} = \begin{pmatrix} \sin(\theta)\cos(\varphi) \\ \sin(\theta)\sin(\varphi) \\ \cos(\theta) \end{pmatrix} \cdot \begin{pmatrix} \cos(cog)sog \\ \sin(cog)sog \\ heave \end{pmatrix} \tag{3}$$

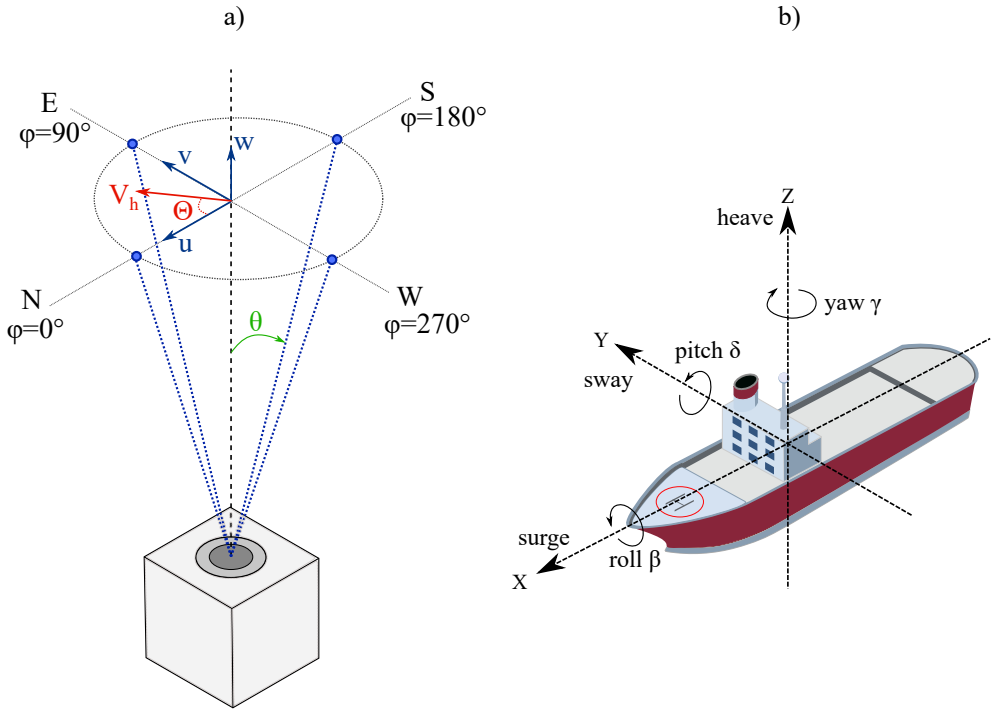

Figure 1. (**a**) Orthogonal frame of the pulsed Doppler lidar assumed in this study. (**b**) Six degrees of freedom motions of the ship.

where *sog* is the speed over ground (vessel speed relative to the earth surface) and *cog* is the course over ground (direction in which the vessel is traveling, measured clockwise from the geographical north).

The rotation matrix included in Equation 2 accounts for the effects of a tilted lidar coordinate system, while the v_{radial}^{ship} term accounts for the translational ship velocity added to or subtracted from the wind velocity projection.

2.2. Simulation cases

In order to simplify the algebra for the derivation of the uncertainty, two different motion scenarios are assumed:

(i) Only translational ship velocity and rotation around the vertical axis are considered $R_{rot} = R_{yaw}(\gamma)$

(ii) Only translational ship velocity and rotation around the horizontal axes are considered $R_{rot} = R_{roll}(\beta) \cdot R_{pitch}(\delta)$

Assuming the meteorological convention for wind direction (wind direction states the direction from which the wind is coming), the horizontal components of the wind vector, u and v, can be expressed in terms of the horizontal wind speed V_h and wind direction Θ:

$$u = -V_h \cos(\Theta) \tag{4}$$

$$v = -V_h \sin(\Theta) \tag{5}$$

By introducing Equations 4 and 5 into 2, applying the corresponding rotation matrix for each motion case, and assuming that the vertical component of the wind speed, w, is very small, and

thus, negligible, the retrieved radial velocity under the two different motion scenarios can be described as:

$$v_{radial}^{meas} = -\sin(\theta) \cdot [V_h \cos(\Theta - \varphi - \gamma) + sog \cos(cog - \varphi - \gamma)] \tag{6}$$

and

$$\begin{aligned} v_{radial}^{meas} = [-V_h \cos(\Theta) - \cos(cog) sog] \cdot [\cos(\delta) \sin(\theta) \cos(\varphi) + \sin(\delta) \cos(\theta)] \\ -[V_h \sin(\Theta) + \sin(cog) sog] \cdot [\sin(\theta)\{\cos(\beta) \sin(\varphi) - \sin(\beta) \sin(\delta) \cos(\varphi)\} + \sin(\beta) \cos(\delta) \cos(\theta)] \end{aligned} \tag{7}$$

for the case i and ii, respectively.

2.3. Assumptions for uncertainty derivations

The following assumptions have been considered for the derivation of the uncertainty model presented in this paper:

- The vertical component of the wind speed and ship velocity (heave) are very small, and therefore, they are not considered in the model derivation.
- We assume horizontal homogeneity of the wind field.
- Impact of wind shear is omitted for the model derivation.
- Time scales of motion and orientation changes are much slower than the reference time scale (defined by the sampling frequency of the lidar device).
- When the ship is moving, *cog* is (approximately) equal to the ship heading.
- The considered uncertainty contributors are independent from each other.

2.4. Derivation of the retrieved radial velocity uncertainty

Applying the law of propagation of uncertainty [11] to Equation 6 and considering that the uncertainty contributors of v_{radial}^{motion} are independent from each other, the combined uncertainty for the case i can be calculated as:

$$u_{v_{radial}^{motion}}^2 = \left(u_\gamma \frac{\partial v_{radial}^{motion}}{\partial \gamma} \right)^2 + \left(u_{sog} \frac{\partial v_{radial}^{motion}}{\partial sog} \right)^2 + \left(u_{cog} \frac{\partial v_{radial}^{motion}}{\partial cog} \right)^2 \tag{8}$$

where $u_{v_{radial}^{meas}}$, u_γ, u_{sog} and u_{cog} are the standard uncertainties of the radial velocity, yaw, speed over ground and course over ground, respectively.

The partial derivatives from Equation 8 are:

$$\frac{\partial v_{radial}^{motion}}{\partial \gamma} = -\sin(\theta) \cdot [V_h \sin(\Theta - \varphi - \gamma) + \sin(cog - \varphi - \gamma) sog] \tag{9}$$

$$\frac{\partial v_{radial}^{motion}}{\partial sog} = -\sin(\theta) \cdot \cos(cog - \varphi - \gamma) \tag{10}$$

$$\frac{\partial v_{radial}^{motion}}{\partial cog} = \sin(\theta) \cdot \sin(cog - \varphi - \gamma) sog \tag{11}$$

The first partial derivative reflects the uncertainty associated with the error when projecting the linear velocities (horizontal wind speed V_h and ship velocity sog) to the lidar beams. As it can be observed, this partial derivative is composed of two different terms. The first one accounts

for the contribution of the error when projecting the horizontal wind speed to the LoS direction; it reaches the maximum when the lidar beam is perpendicular to the wind direction. The second one accounts for the contribution of the projection of the ship horizontal velocity, reaching a maximum when the lidar beam is perpendicular to the ship direction *cog*. The logic behind this is the higher sensitivity of the V_h and *sog* projection in the LoS direction when the beam is perpendicular to the corresponding linear velocity. Analogously, Equation 11 also expresses the error of the *sog* projection, but not the one corresponding to the V_h projection. Because of this, we expect a magnification in the sensitivity of the radial velocity uncertainties to variations in the ship velocity. Equation 10 reaches minimum values when the lidar beams are perpendicular to the ship course over ground, since those beams are not "seeing" the translational component added by the ship velocity.

Introducing these partial derivatives in Equation 8 we get the final expression of the radial velocity uncertainties for the case i.

Following the same procedure, and equally applying the law of propagation of uncertainty to Equation 7, the combined radial velocity uncertainty for the case ii can be derived as:

$$u^2_{v^{motion}_{radial}} = \left(u_\beta \frac{\partial v^{motion}_{radial}}{\partial \beta}\right)^2 + \left(u_\delta \frac{\partial v^{motion}_{radial}}{\partial \delta}\right)^2 + \left(u_{sog} \frac{\partial v^{motion}_{radial}}{\partial sog}\right)^2 + \left(u_{cog} \frac{\partial v^{motion}_{radial}}{\partial cog}\right)^2 \quad (12)$$

with u_β and u_δ being the standard uncertainty of the roll and pitch, respectively. Due to the required space and to improve paper readability, partial derivatives from Equation 12 are omitted from the main body of the text. However, they can be found in the Appendix A.

2.5. Derivation of the horizontal wind speed and direction uncertainty

As a consequence of the motion effects on the retrieved radial velocity, ship-based lidar observations require the application of a motion correction algorithm to take these motion effects out from the measurements. The reader may refer to previous literature for further information regarding potential approaches for this purpose (e.g. [12, 13, 14, 15]). In this study, we applied the methodology explained in [5], which allows to calculate the decontaminated wind speed $\vec{u}$ applying the following mathematical expression:

$$\vec{u} = R_{rot} \cdot \vec{u}_{motion} + \vec{u}_{ship} \quad (13)$$

Using radial velocities measured at different azimuth angles and a Doppler beam swinging (DBS) algorithm [16], the horizontal component of the motion-contaminated wind speed vector $\vec{u}_{motion}$ is calculated as:

$$u_{motion} = \frac{v^{motion,N}_{radial} - v^{motion,S}_{radial}}{2\sin(\theta)} \quad (14)$$

$$v_{motion} = \frac{v^{motion,E}_{radial} - v^{motion,W}_{radial}}{2\sin(\theta)} \quad (15)$$

Introducing Equations 14 and 15 into Equation 13, the corrected wind speed vector for the case i is expressed as:

$$\vec{u} = \frac{1}{2\sin(\theta)} \begin{pmatrix} \cos(\gamma)(v^{motion,N}_{radial} - v^{motion,S}_{radial}) - \sin(\gamma)(v^{motion,E}_{radial} - v^{motion,W}_{radial}) + 2\sin(\theta)\cos(cog)sog \\ \sin(\gamma)(v^{motion,N}_{radial} - v^{motion,S}_{radial}) + \cos(\gamma)(v^{motion,E}_{radial} - v^{motion,W}_{radial}) + 2\sin(\theta)\sin(cog)sog \end{pmatrix} \quad (16)$$

Reader may notice that the wind speed vector for case *ii* has been omitted for the sake of brevity. However, it can be calculated following the same procedure. The horizontal wind speed is calculated as the root squared sum of $\vec{u}$ horizontal components:

$$V_h = \frac{1}{2\sin(\theta)}\Big\{(v^N_{radial} - v^S_{radial})^2 + (v^E_{radial} - v^W_{radial})^2 + 4\sin^2(\theta)sog^2 \\ +4\sin(\theta)sog[(v^N_{radial} - v^S_{radial})\cos(\gamma - cog) + (v^E_{radial} - v^W_{radial})\sin(cog - \gamma)]\Big\}^{1/2} \tag{17}$$

Whereas the wind direction can be mathematically obtained as:

$$\Theta = \tan^{-1}\left(\frac{v}{u}\right) \tag{18}$$

Finally, the uncertainty of the horizontal wind speed u_{V_h} and the wind direction u_Θ can be derived applying the law of propagation of uncertainty to Equations 17 and 18, respectively, and calculating the partial derivatives for the radial velocities calculated at the four lidar azimuth directions:

$$u^2_{V_h} = \sum_{i=0}^{n}\left(U_{v^{motion,i}_{radial}}\frac{\partial V_h}{\partial v^{motion,i}_{radial}}\right) \tag{19}$$

$$u^2_{\Theta} = \sum_{i=0}^{n}\left(U_{v^{motion,i}_{radial}}\frac{\partial \Theta}{\partial v^{motion,i}_{radial}}\right) \tag{20}$$

where n is the number of beams of the considered lidar. The resulting partial derivatives for cases i and ii are found, again, in Appendix A.

3. Results

This section presents the results of the simulated lidar wind speed and direction uncertainties. First, we evaluate the uncertainty sensitivity to the lidar device orientation regarding the ship direction. Later, we study the influence of the translational vessel velocity, and finally, we conclude this section with an analysis of the ship tilting effect in the derived measurement uncertainties.

3.1. Sensitivity to lidar misalignment

During the deployment of lidar devices, we must carefully consider the orientation of the system. When a fixed device is employed, the general recommended practice is to orientate the lidar north beam ($\varphi = 0°$) towards the geographical north to reduce the obtained uncertainty levels. Nonetheless, when considering ship-mounted lidars, this recommendation is no longer effective due to the constant variations of the ship heading. As an alternative, the relative orientation of the lidar regarding the ship is a more appropriate parameter to consider when deploying lidars on vessels. In this paper, we will refer to this relative orientation as misalignment, defined as the clockwise measured angle between the bow-stern ship axis and the lidar north beam.

Figure 2 shows the horizontal wind speed uncertainty maps for four different ship directions and as a function of the lidar misalignment. The results show a clear dependency of the uncertainty on the relative direction between the wind and the ship heading. As can be observed, the wind directions parallel to the ship heading, but with an offset of 180°, are the regions showing lower levels of uncertainty. As an example, when considering a ship orientation of 45°, we will observe the most certain wind estimations at wind directions near to 225°. This can be elucidated by

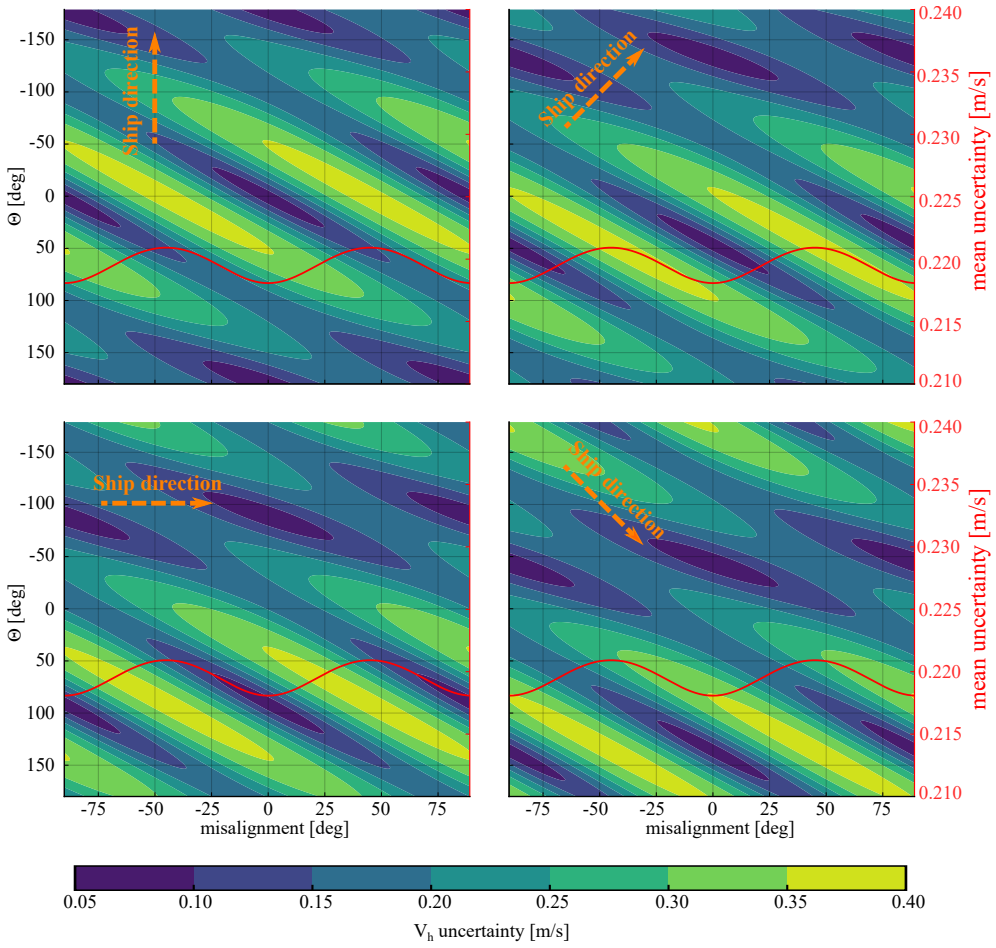

Figure 2. V_h uncertainty maps depending on wind direction (y axis) and misalignment (x axis). Four different ship directions are considered (0°, 45°, 90°and 135°). For each case, the mean uncertainty averaged over all the wind directions is represented by the red line.

highlighting that, under these conditions, two lidar beams are parallel to the wind direction and ship linear velocity, resulting in a smaller total sensitivity of their projection on the four lidar beams. When looking at the overall uncertainty averaged over all the wind directions (red lines in Figure 2), the most certain retrievals appear when the lidar misalignment is equal to 0°or ±90°. On the contrary, maximum uncertainties are expected for misalignment angles of ±45°. This is a consequence of the scanning geometry of the considered lidar, with four laser beams separated 90°from the adjacent beams and resulting in minimum uncertainties for those misalignment angles that coincide with the four azimuth directions of the considered lidar beams. Therefore, two main conclusions can be derived. First, the correct alignment of the lidar beams regarding the ship's bow-stern axis would reduce the uncertainties of ship-based measurement campaigns. Second, increasing the number of beams would also help to decrease the total uncertainty of the wind speed measurements.

Figure 3 shows the wind direction uncertainty for several ship directions, as well as the overall average. As can be observed, all the lines for different *cog* values follow a sinusoidal line which reaches a maximum at those misalignment values equal to *cog*±90°, and a minimum for *cog*±45°. However, when looking at the average uncertainty over all the *cog* values, the optimal (i.e. lowest) uncertainty is obtained for a misalignment of around 0°.

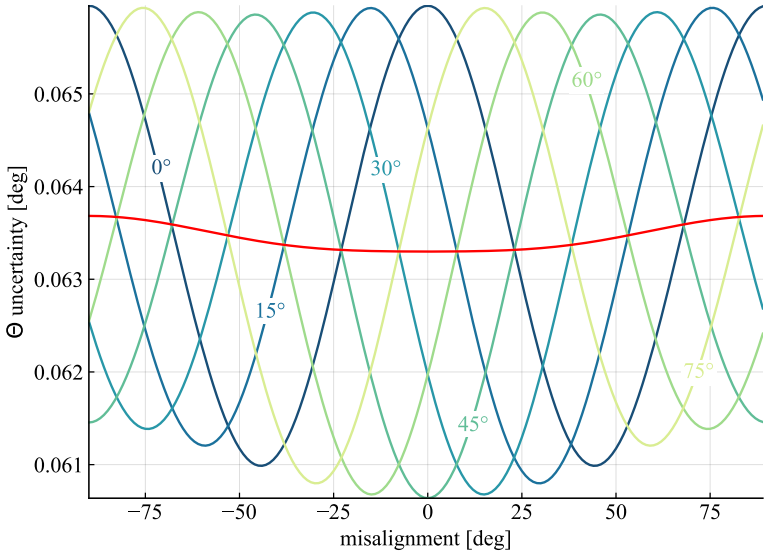

Figure 3. Wind direction (Θ) uncertainty as a function of lidar misalignment. Each line on the blue-to-green scale indicates the average uncertainty for the indicated ship direction (*cog*). The red line represents the overall mean uncertainty for all the *cog* values.

It must be mentioned that the overall uncertainty values (red lines in Figures 2 and 3) are calculated for a constant half cone opening angle of 28°. Nevertheless, additional evaluations show that these values are constant for θ angles in (0°, 90°). Consequently, for this particular case (ship not tilting), the half cone opening angle does not significantly influence the measurement uncertainties.

3.2. Influence of ship translational motions

Ship translational motions shift the lidar detected Doppler frequency due to the change in the relative velocities between the emitted lidar pulse and the backscatters. Consequently, the retrieved radial velocities are contaminated by a velocity magnitude proportional to the vessel's linear speed. Figure 4a shows how the horizontal ship velocity influences the horizontal wind speed uncertainty. As expected, higher values of speed over ground and horizontal wind velocities raise the uncertainty values. It is even more interesting to compare how the uncertainty changes when considering a constant value of wind speed against those changes associated with a constant value of *sog*. On the one hand, it can be observed that when considering a constant ship velocity, the uncertainty remains almost constant over the whole range of horizontal wind velocities. On the other hand, for a constant horizontal wind speed, small variances in the ship velocity trigger fast changes in the uncertainty levels. Therefore, wind speed uncertainties are more sensitive to fluctuations in the ship's velocity than to those same fluctuations in the wind speed.

In order to evaluate the effect of the relation between the ship velocity and the horizontal wind speed in the uncertainty of the measurements, we defined the velocity ratio VR parameter, expressed as:

$$VR = \frac{\text{sog}}{V_h} \tag{21}$$

In Figure 4a, three different velocity ratios (0.5, 1, and 2) are indicated by the dashed blue,

black, and red lines. As can be observed, higher ship velocities regarding a considered horizontal wind speed are associated with higher uncertainties. Accordingly, maintaining low velocity ratios during the execution of ship based lidar campaigns would contribute to reducing the uncertainty of the obtained lidar measurements.

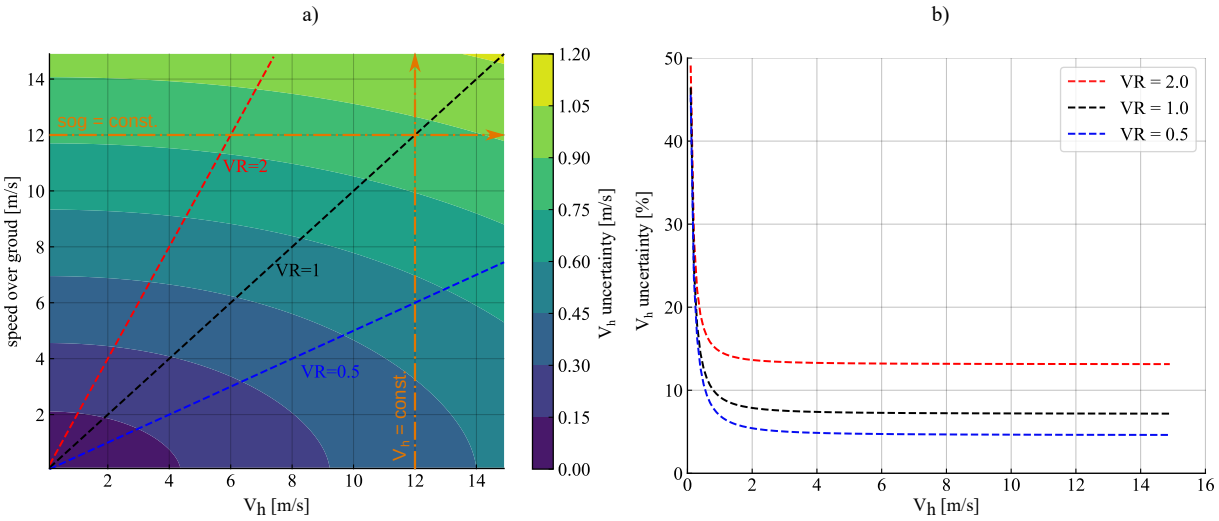

Figure 4. (**a**) V_h uncertainty map for different ship and horizontal wind speed velocities (averaged over all wind directions). The three dashed lines indicate values for velocity ratios of 0.5, 1 and 2. The dash-dotted orange lines indicate the uncertainty evolution for constant wind speed and ship velocity. (**b**) V_h relative (to horizontal wind speed) uncertainty for different velocity ratios.

The influence of the velocity ratio is also evidenced in Figure 4b, where the relative uncertainty for the three aforementioned velocity ratios is presented. Small wind speeds lead to considerably higher values of uncertainty independently of the velocity ratio and reaching relative uncertainties of almost 50% in any of the three considered cases. However, when the wind speed increases above 2 m/s, the uncertainty shows a clear dependency on the velocity ratio considered, being this higher with higher ratios. It is striking that uncertainty levels remain almost constant for a considered velocity ratio independently of the horizontal wind speed, and gradually increase with the velocity ratio.

The effects of the velocity ratio in the wind direction uncertainties have been also evaluated. However, results show a negligible influence of the VR in the wind direction uncertainty levels, and therefore, they have been omitted from this paper.

3.3. Effects of ship tilting

Ship tilting alters the lidar's scanning geometry, modifying the zenith angle of the lidar beams, and thus, altering the sensitivity of the wind and ship velocities' projections in the LoS directions. Figure 5 shows the radial velocity uncertainties for different pitch and roll angles, assuming that the vessel and the lidar are perfectly aligned to the geographical north. As can be observed, lidar tilting differently influences the radial velocity uncertainties depending on the relative direction between the laser beam and the wind direction. For example, a positive rotation around the x axis (ship bow tilting down, blue lines in Figure 5) leads to a north lidar beam ($\varphi = 0°$) more tilted towards the horizontal component of the wind speed, and thus, to a smaller horizontal wind speed sensitivity which translates into a lower uncertainty. On the contrary, the same pitch angle causes the south beam to be more perpendicular to the horizontal wind speed, and thus,

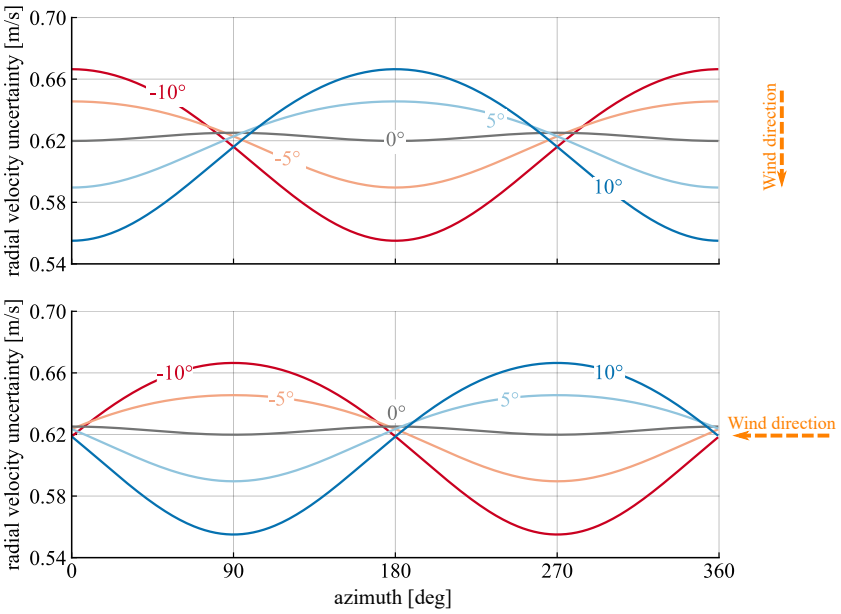

Figure 5. Radial velocity uncertainties for different pitch (top) and roll (bottom) angles. The orange arrows at the right side of the figures indicate the considered wind direction for each case.

to an increase in the uncertainty compared to the non-tilted situation (grey line in Figure 5). It must be noted that the decrease and increase in the uncertainty of the north and south beams, respectively, are one-to-one proportional, and thus, the total uncertainty when considering these two beams remains invariable. Nevertheless, the effect in the beams perpendicular to the wind direction is different. When the ship is tilted, independently of the tilting sign, both beams are more directed towards the horizontal component of the wind speed, and then, a reduction in their uncertainty is reflected. This reduction is equal for the two perpendicular beams and more prominent for higher tilting conditions. Because of this, higher tilting values generate lower uncertainty values when considering the four beams.

The uncertainty reduction with tilting can be also observed when deriving the horizontal wind speed and direction uncertainty, as presented in Figure 6. Although the uncertainty sensitivity is not very pronounced, we can clearly identify an uncertainty reduction trend when moving towards more pronounced tilting situations.

Finally, the influence of the half cone opening angle is evaluated in Figure 7, where the total wind speed and direction uncertainty has been calculated for θ angles between [5°, 85°]. Contrary to what is stated in Section 3.1, both the wind speed and direction uncertainty shows an exponential decrease when increasing the half cone opening angle. The reasoning for this can be found in the fact that, increasing θ increments the effect shown in Figure 5, with those perpendicular beams more directed toward the horizontal wind speed and thus, a total smaller uncertainty when considering the four beams.

4. Conclusions and Outlook

In this study, uncertainties from ship-based lidar measurements have been simulated through the derivation of an uncertainty model for ship-mounted pulsed Doppler lidars. The model has been developed analytically and under the consideration of several assumptions to keep the mathematical complexity manageable. However, it provides meaningful insights into the sensitivity of ship-mounted lidar measurements to relevant parameters associated with these sorts of systems.

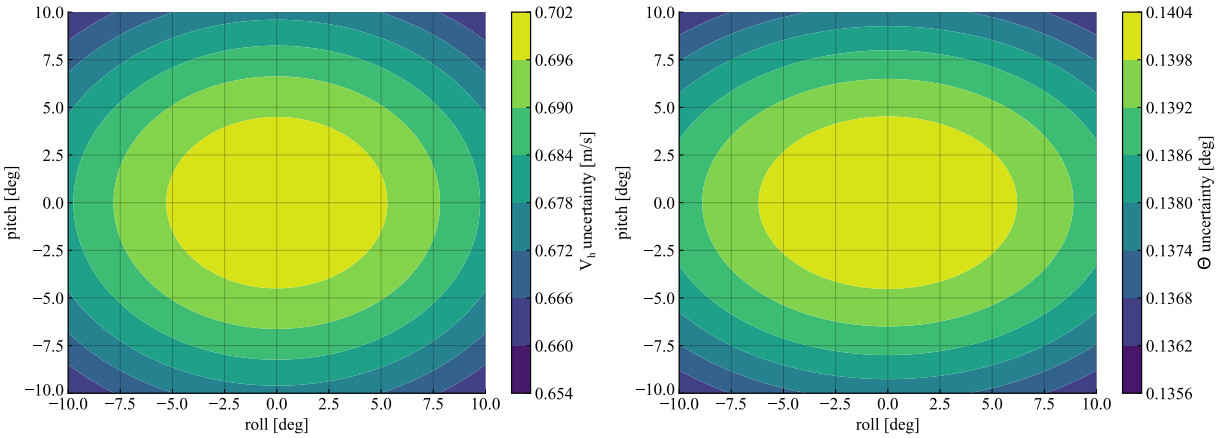

Figure 6. Total wind speed and direction uncertainty (averaged over all wind directions) maps for wind speed (left) and direction (right) depending on ship tilting.

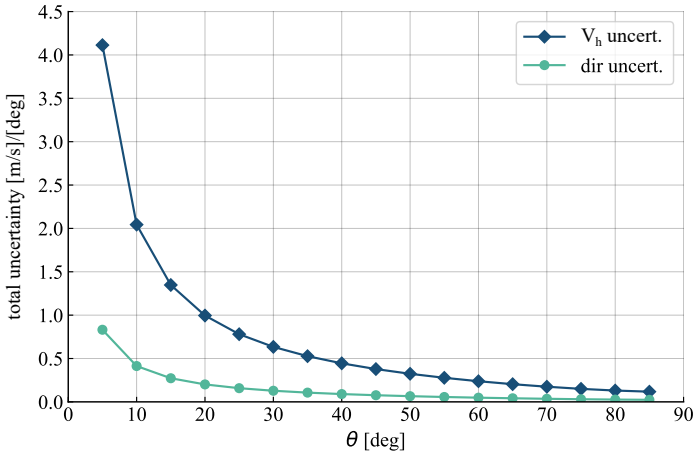

Figure 7. Total wind speed and direction uncertainty for several half cone opening angles.

First, the correct alignment of the lidar and the ship has demonstrated to increase the overall reliability of the measurements, both in terms of wind speed and wind direction. For the studied case, the perfect alignment of the ship and the lidar device would achieve a decrease of around 2% in the total uncertainty compared to the worst case scenario (45° misalignment). Additionally, it could be derived that increasing the number of lidar beams could benefit the uncertainty levels obtained. Secondly, the results demonstrated the effectiveness of maintaining low-velocity ratios in reducing wind speed uncertainties, for instance, by using slow ships for executing new campaigns. Finally, tilting conditions positively contribute to decreasing the uncertainty levels associated with the observations compared to the non-tilted case, with reductions of up to 7% and 3.5% for the wind speed and direction, respectively.

In conclusion, the presented results not only give a quantitative understanding of the confidence associated with ship-based lidar measurements but also bring practical information about the optimal technology setup for the execution of future campaigns. For all this, this work represents a first step towards the development of a reproducible methodology for ship-based lidar systems. Nevertheless, further efforts are needed to extend the model presented here by introducing

additional variables that may also play a significant role in the uncertainty levels, such as the wind shear or vertical component velocities. Finally, to validate the reliability and robustness of the model, a comparison against real observational data is required and will be the goal of future related investigations.

Acknowledgments
This work is founded by the European Union's Horizon 2020 research and innovation program under the Marie Skłodowska-Curie Grant Agreement No. 858358 (LIKE—Lidar Knowledge Europe).

Appendix A. Partial derivatives for uncertainty derivation

Appendix A.1. Partial derivatives of radial velocity for case ii
The partial derivatives from Equation 12 are:

$$\frac{\partial v_{radial}^{motion}}{\partial \beta} = [V_h \sin(\Theta) + \sin(cog)sog] \\ [\cos(\beta)(\sin(\delta)\cos(\varphi)\sin(\theta) - \cos(\delta)\cos(\theta)) + \sin(\beta)\sin(\varphi)\sin(\theta)] \tag{A.1}$$

$$\frac{\partial v_{radial}^{motion}}{\partial \delta} = [-V_h \sin(\Theta) - \sin(cog)sog][-\sin(\beta)\cos(\theta)\sin(\delta) - \sin(\beta)\cos(\varphi)\sin(\theta)\cos(\delta)] \\ +[-V_h \cos(\Theta) - \cos(cog)sog][\cos(\theta)\cos(\delta) - \cos(\varphi)\sin(\theta)\sin(\delta)] \tag{A.2}$$

$$\frac{\partial v_{radial}^{motion}}{\partial sog} = -\sin(cog)[\sin(\theta)(\cos(\beta)\sin(\varphi) - \sin(\beta)\cos(\varphi)\sin(\delta)) + \sin(\beta)\cos(\delta)\cos(\theta)] \\ +\cos(cog)[\cos(\delta)\cos(\varphi)\sin(\theta) + \sin(\delta)\cos(\theta)] \tag{A.3}$$

$$\frac{\partial v_{radial}^{motion}}{\partial cog} = -\cos(cog)sog[\sin(\theta)(\cos(\beta)\sin(\varphi) - \sin(\beta)\cos(\varphi)\sin(\delta)) + \sin(\beta)\cos(\delta)\cos(\theta)] \\ +\sin(cog)sog[\cos(\delta)\cos(\varphi)\sin(\theta) + \sin(\delta)\cos(\theta)] \tag{A.4}$$

Appendix A.2. Partial derivatives for horizontal wind speed uncertainties
The partial derivatives in Equation 19 for the case i are:

$$\frac{\partial V_h}{\partial v_{radial}^{motion,N}} = \frac{v_{radial}^{motion,N} - v_{radial}^{motion,S} + 2\sin(\theta)\cos(cog-\gamma)sog}{4V_h \sin^2(\theta)} \tag{A.5}$$

$$\frac{\partial V_h}{\partial v_{radial}^{motion,E}} = \frac{v_{radial}^{motion,E} - v_{radial}^{motion,W} + 2\sin(\theta)\cos(cog-\gamma)sog}{4V_h \sin^2(\theta)} \tag{A.6}$$

$$\frac{\partial V_h}{\partial v_{radial}^{motion,S}} = \frac{v_{radial}^{motion,S} - v_{radial}^{motion,N} - 2\sin(\theta)\cos(cog-\gamma)sog}{4V_h \sin^2(\theta)} \tag{A.7}$$

$$\frac{\partial V_h}{\partial v_{radial}^{motion,W}} = \frac{v_{radial}^{motion,W} - v_{radial}^{motion,E} - 2\sin(\theta)\cos(cog-\gamma)sog}{4V_h \sin^2(\theta)} \tag{A.8}$$

Whereas, for the case *ii*:

$$\frac{\partial V_h}{\partial v_{radial}^{motion,N}} = \frac{1}{4V_h \sin^2(\theta)} \Big\{ 2\sin(\theta) sog(\sin(\beta)\sin(cog)\sin(\delta) + \cos(cog)\cos(\delta)) - \sin(\beta)\cos(\beta)\sin(\delta)(v_{radial}^{motion,E} - v_{radial}^{motion,W}) + (v_{radial}^{motion,N} - v_{radial}^{motion,S})(\sin^2(\beta)\sin^2(\delta) + \cos^2(\delta)) \Big\} \tag{A.9}$$

$$\frac{\partial V_h}{\partial v_{radial}^{motion,E}} = \frac{1}{4V_h \sin^2(\theta)} \Big\{ 2\cos(\beta)\sin(cog)\sin(\theta) sog - \sin(\beta)\cos(\beta)\sin(\delta)(v_{radial}^{motion,N} - v_{radial}^{motion,S}) + \cos^2(\beta)(v_{radial}^{motion,E} - v_{radial}^{motion,W}) \Big\} \tag{A.10}$$

$$\frac{\partial V_h}{\partial v_{radial}^{motion,S}} = \frac{1}{4V_h \sin^2(\theta)} \Big\{ -2\sin(\theta) sog(\sin(\beta)\sin(cog)\sin(\delta) + \cos(cog)\cos(\delta)) + \sin(\beta)\cos(\beta)\sin(\delta)(v_{radial}^{motion,E} - v_{radial}^{motion,W}) - (v_{radial}^{motion,N} - v_{radial}^{motion,S})(\sin^2(\beta)\sin^2(\delta) + \cos^2(\delta)) \Big\} \tag{A.11}$$

$$\frac{\partial V_h}{\partial v_{radial}^{motion,W}} = \frac{1}{4V_h \sin^2(\theta)} \Big\{ -2\cos(\beta)\sin(cog)\sin(\theta) sog + \sin(\beta)\cos(\beta)\sin(\delta)(v_{radial}^{motion,N} - v_{radial}^{motion,S}) - \cos^2(\beta)(v_{radial}^{motion,E} - v_{radial}^{motion,W}) \Big\} \tag{A.12}$$

Appendix A.3. Partial derivatives for wind direction uncertainties
The partial derivatives in Equation 20 for the case i are:

$$\frac{\partial \Theta}{\partial v_{radial}^{motion,N}} = \frac{\sin(\Theta - \gamma)}{2V_h \sin(\theta)} \tag{A.13}$$

$$\frac{\partial \Theta}{\partial v_{radial}^{motion,E}} = \frac{-\cos(\Theta - \gamma)}{2V_h \sin(\theta)} \tag{A.14}$$

$$\frac{\partial \Theta}{\partial v_{radial}^{motion,S}} = \frac{\sin(\Theta + \gamma)}{2V_h \sin(\theta)} \tag{A.15}$$

$$\frac{\partial \Theta}{\partial v_{radial}^{motion,W}} = \frac{\cos(\Theta - \gamma)}{2V_h \sin(\theta)} \tag{A.16}$$

Whereas, for the case *ii*:

$$\frac{\partial \Theta}{\partial v_{radial}^{motion,N}} = \frac{\sin(\Theta)\cos(\delta) + \cos(\Theta)\sin(\beta)\sin(\delta)}{2V_h \sin(\theta)} \tag{A.17}$$

$$\frac{\partial \Theta}{\partial v_{radial}^{motion,E}} = \frac{-\cos(\Theta)\cos(\beta)}{2V_h \sin(\theta)} \tag{A.18}$$

$$\frac{\partial \Theta}{\partial v_{radial}^{motion,S}} = \frac{-\sin(\Theta)\cos(\delta) - \cos(\Theta)\sin(\beta)\sin(\delta)}{2V_h \sin(\theta)} \tag{A.19}$$

$$\frac{\partial \Theta}{\partial v_{radial}^{motion,W}} = \frac{\cos(\Theta)\cos(\beta)}{2V_h \sin(\theta)} \tag{A.20}$$

Appendix B. Parametrization of cases

In order to evaluate the uncertainty sensitivity, the model has been parametrized with the values of the intrinsic uncertainties and the evaluated variables. For each of the three subsections in Section 3, the parametrization of the model is included in the following tables:

Table B1. Parametrization of the model in Subsection 3.1.

Parameter	Value	Parameter	Value
V_h	5 m/s		
Θ	[0°- 360°]		
sog	2 m/s	u_{sog}	0.1 m/s
cog	[0°- 360°]	u_{cog}	0.1°
yaw	[0°- 360°]	u_{γ}	0.1°
θ	28°	u_{θ}	0.1°
R_{rot}	R_{yaw}		

Table B2. Parametrization of the model in Subsection 3.2.

Parameter	Value	Parameter	Value
V_h	[0-15] m/s		
Θ	[0°- 360°]		
sog	[0-15] m/s	u_{sog}	0.1 m/s
cog	0°	u_{cog}	0.1°
yaw	0°	u_{γ}	0.1°
θ	28°	u_{θ}	0.1°
R_{rot}	R_{yaw}		

Table B3. Parametrization of the model in Subsection 3.3.

Parameter	Value	Parameter	Value
V_h	5 m/s		
Θ	[0°- 360°]		
sog	2 m/s	u_{sog}	0.1 m/s
cog	0°	u_{cog}	0.1°
θ	28°	u_θ	0.1°
δ	[-10°- 10°]	u_δ	0.1°
β	[-10°- 10°]	u_β	0.1°
R_{rot}	$R_{roll}R_{pitch}$		

References

[1] Soares C G 2015 *Renewable energies offshore: Proc. of the 1st Int. Conf. on Renewable Energies Offshore, Lisbon, Portugal, 24-26 November 2014 / editor, C. Guedes Soares* (Boca Raton, FL: CRC Press) ISBN 9781138028715
[2] Gottschall J, Gribben B, Stein D and Würth I 2017 *Wiley Interdiscip. Rev.: Energy Environ.* **6** e250 ISSN 20418396
[3] Gottschall J, Catalano E, Dörenkämper M and Witha B 2018 *Remote Sens.* **10** 1620
[4] Achtert P, Brooks I M, Brooks B J, Moat B I, Prytherch J, Persson P O G and Tjernström M 2015 *Atmos. Meas. Tech.* **8** 4993–5007
[5] G Wolken-Möhlmann, J Gottschall and B Lange 2014 *Energy Procedia* **53** ISSN 18766102
[6] Catalano E 2017 Assessment of offshore wind resources through measurements from a ship-based lidar system Master thesis
[7] Rubio H, Kühn M and Gottschall J 2022 *In preparation for Wind Energy Sci.*
[8] Pichugina Y L, Brewer W A, Banta R M, Choukulkar A, Clack C T M, Marquis M C, McCarty B J, Weickmann A M, Sandberg S P, Marchbanks R D and Hardesty R M 2017 *Wind Energy* **20** 987–1002 ISSN 10954244
[9] Gottschall J and Witha B 2019 The ferry lidar experiment and benchmark
[10] The Carbon Trust 2018 Carbon trust offshore wind accelerator roadmap for the commercial acceptance of floating lidar technology: Version 2.0
[11] Joint Committee for Guides in Metrology 2008 Evaluation of measurement data — Guide to the expression of uncertainty in measurement
[12] Zhai X, Wu S, Liu B, Song X and Yin J 2018 *Atmos. Meas. Tech.* **11** 1313–1331
[13] Zentek R, Kohnemann S H E and Heinemann G 2018 *Atmos. Meas. Tech.* **11** 5781–5795
[14] Gutiérrez Antuñano M Á 2019 *Doppler wind LIDAR systems data processing and applications: An overview towards developing the new generation of wind remote-sensing sensors for off-shore wind farms* Ph.D. thesis
[15] Kelberlau F, Neshaug V, Lønseth L, Bracchi T and Mann J 2020 *Remote Sens.* **12** 898
[16] Werner C and Streicher J 2005 *Lidar: Range-Resolved Optical Remote Sensing of the Atmosphere* Series in optical sciences (Springer) URL `https://elib.dlr.de/51539/`